Triboelectric Nanogenerator Enhanced Schottky Nanowire Sensor for Highly Sensitive Ethanol Detection

Jianping Meng,[∇] Hu Li,[∇] Luming Zhao, Junfeng Lu, Caofeng Pan, Yan Zhang, and Zhou Li*

Cite This: https://dx.doi.org/10.1021/acs.nanolett.0c01063

Read Online

ACCESS | Metrics & More | Article Recommendations | Supporting Information

ABSTRACT: Highly sensitive ethanol sensors are important for environmental and industrial monitoring. In our work, we demonstrate a method to enhance the response of a Schottky sensor based on a ZnO nano/microwire (NMW) by triboelectric nanogenerator (TENG). Via lowering the Schottky barrier height (SBH) via the high voltage from TENG, the response of the sensor is enhanced by 139% for 100 ppm ethanol. This method accelerates the recovery process. The high voltage from TENG produces a high intensity electric field to drive diffusion of the oxygen vacancies in ZnO NMW toward to the junction area around the interface. It is equivalent to applying the reverse voltage on the Schottky junction, which leads to the increase of depletion width. More chemisorbed oxygen on the depletion region is consumed once the ethanol gas is injected into the chamber, which improves the response of the ethanol sensor. This study provides a new, simple, and effective method to improve the sensor response.

KEYWORDS: Ethanol sensor, Schottky contact, Triboelectric nanogenerator, ZnO nanowire
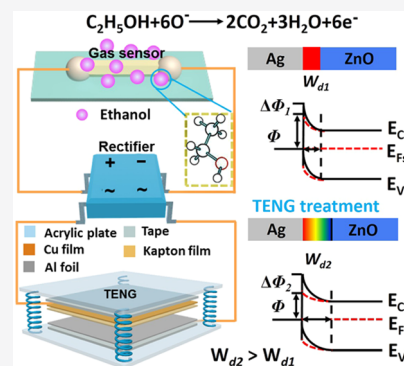
INTRODUCTION

As a common volatile chemical in industrial productions, the control and monitoring of ethanol are vital for safety and in drunk driving testing.[1−3] Ethanol sensors play an important role in our daily life in avoiding the potential property damage and personal injury due to the abuse of ethanol.[4,5]

The surface-to-volume ratio of the material used in fabricating the gas sensor is an important factor because the reaction between the gas and the material mainly occurs on the surface.[6] One-dimensional nanomaterials have attracted much research attention because of their high surface-to-volume ratio. Of these, ZnO as an n-type semiconductor is a key member for gas sensors due to its superiority of low cost, low toxicity, good thermal stability, and high electron mobility.[7] Generally, the Schottky junction is preferential when ZnO nano/microwire (NMW) is used for the gas sensor.[8] Extensive work has been done to improve the sensor's sensitivity, selectivity, speed (response/recovery time), and stability.[5] Compared with an Ohmic-contacted sensor, the Schottky-contacted sensor has a higher sensitivity.[8] The sensitivity can be further improved by tuning the Schottky barrier height (SBH).[9−11] Piezopotential is an effective method to tune SBH. The change of SBH is attributed to the internal electric field which is formed by the piezopotential when a stress is applied to the piezoelectric materials.[12−15] The generation of a piezopotential is based on the deformation of a piezoelectric material, and the risk of potential fracture to piezoelectric materials may limit their application widely. Tuning SBH can also be achieved by generating the internal electric field via applying an external voltage.

The high voltage and low current render the triboelectric nanogenerator (TENG) as a high voltage power source with safety, low cost, and portability.[16−20] Compared with a commercial voltage source, TENG can be assembled easily using any two different materials in laboratories, which can lower the manufacturing cost greatly. Additionally, TENG has four basic working modes, and it broadens the source of external voltage by a facile triboelectric device. For application scenarios of high voltage, the high voltage of a commercial power source usually accompanies a high unsafe current (amperes), but TENG exhibits a low output current (micro-amps) even at a high voltage. Here, the preferential TENG is used to tune SBH to improve the performance of an ethanol sensor of ZnO NMW. The comprehensive system of the highly sensitive ethanol sensor is designed. An interesting phenomenon is found that the SBH of the ZnO NMW(n-type)-based Schottky sensor can be lowered by the positive voltage of TENG. A theoretical model is proposed to explain this phenomenon. The response of the ethanol sensor based on ZnO NMW is improved for the concentration range of 5 to 200 ppm. This study provides a new, simple, and effective
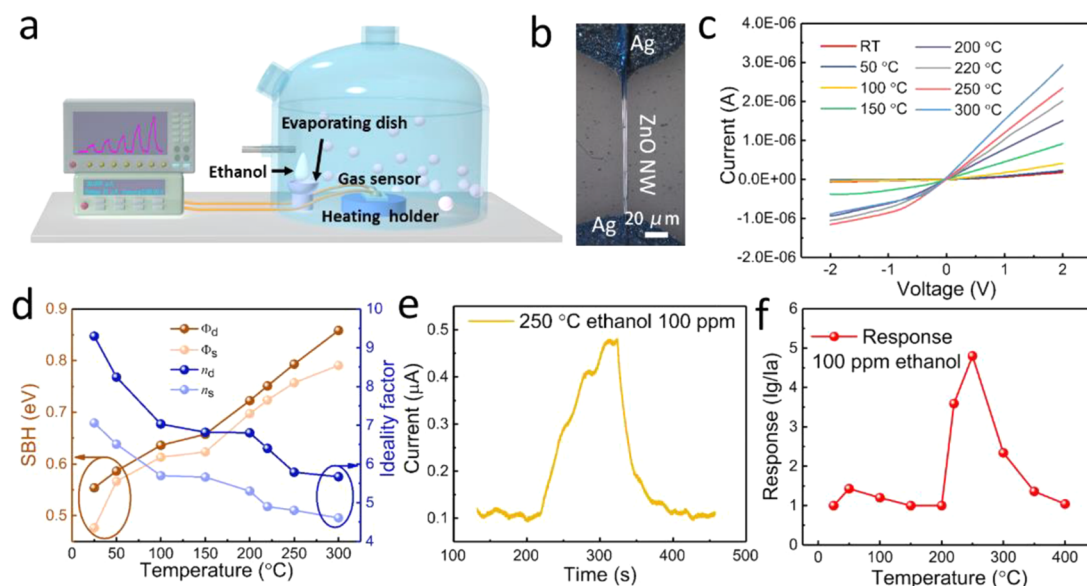
Figure 1. Measurement process of gas sensing and the influence of temperature to the ZnO NMW ethanol sensor. (a) Schematic diagram of experiment setup for investigating the ethanol sensor based on the ZnO NMW. (b) Optical microscopy image of a ZnO NMW ethanol sensor. (c) I−V curve of ethanol sensor at different temperatures. (d) Variation in SBH and ideality factor with the operating temperature. (e) The response curves of ethanol sensor for 100 ppm ethanol at 250 °C. (f) Response of 100 ppm ethanol at different temperatures.
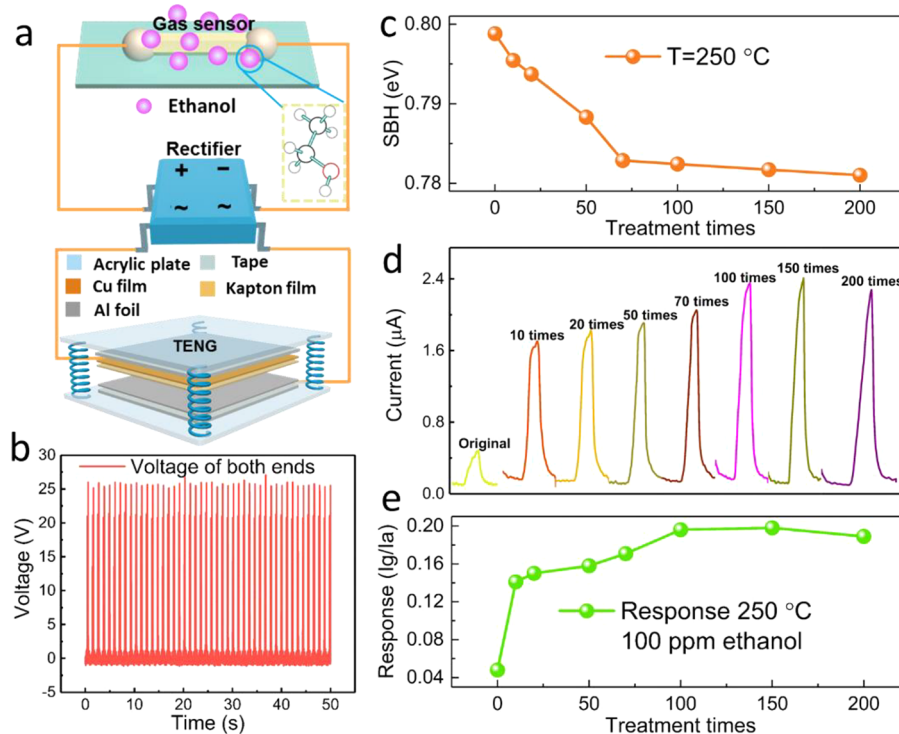

Figure 2. Influence of TENG on an ethanol sensor based on ZnO NMW. (a) Schematic diagram of experiment setup of the ethanol sensor treated by TENG. (b) The applied voltage of TENG on the ethanol sensor based on the ZnO NMW Schottky junction. (c) SBH of the ethanol sensor based on the ZnO NMW Schottky junction as a function of treatment times. (d) The response curves of the ethanol sensor before and after TENG treatment to 100 ppm ethanol at 250 °C. (e) The response of ethanol sensor based on ZnO NMW after TENG treatment for different times.

method to improve the response of Schottky-junction-based sensors.

RESULTS AND DISCUSSION

The ethanol sensor based on the ZnO NMW was placed on a heating holder. Liquid ethanol was injected into the chamber. Then, the liquid ethanol was evaporated into a gas for measurement (Figure 1a). The optical microscopy image of the gas sensor is shown in Figure 1b. The current increases as the temperature increases (Figure 1c). Schottky characteristics become less conspicuous as the temperature increases. The increase of temperature will produce more high-energy electrons, which worsens the rectifying function of the ethanol sensor.[21−23] The ideality factors of source and drain electrodes
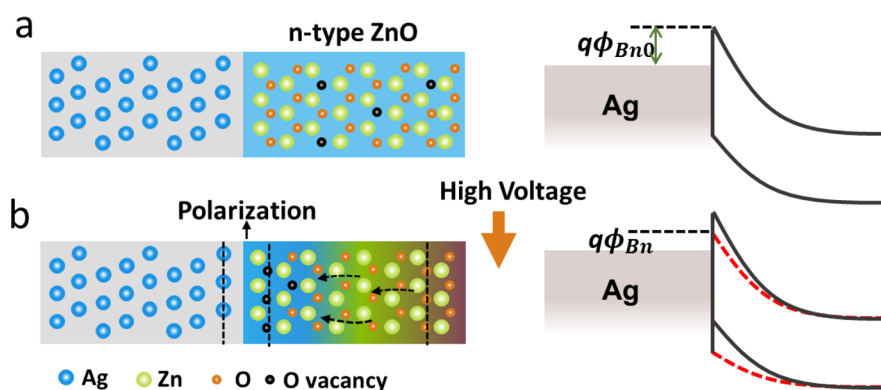
Figure 3. Polarization model and schematic diagram of SBH variation. (a) The model of an M-S contact consisted of Ag and n-type ZnO. The initial state is a Schottky contact. (b) Oxygen vacancies are driven by the positive high voltage of TENG, and the positive charges are aggregated at the interface; SBH is lowered from ϕ_{Bn0} to ϕ_{Bn} due to polarization.

are decreased with the increase of temperature, whereas the SBH is increased (Figure 1d). Assuming that the thermionic emission is the main dominant mechanism, this phenomenon is in accordance with the temperature effect on the Schottky junction.[21−23] Figure 1e is the response curve of 100 ppm ethanol at 250 °C. The other response curves at different temperatures can be observed in Figure S1. Based on the response curve, the response value at different temperatures is plotted in Figure 1f. When the temperature is no less than 200 °C, the response fluctuates within a narrow range (i.e., 1−1.5). Then, the response increases to 4.8 at 250 °C. Over this temperature, the response decreases. In air, the chemisorbed oxygen on the surface of ZnO NMW will accept the electrons from ZnO. The surface of ZnO NMW forms an electron-depletion layer. The chemisorbed oxygen is turned into negatively charged species (including O_2^-, O^-, or O^{2-}).[24,25] At low temperature (<100 °C), the main charged species is O_2^-. It has low reactivity, and there is little reactive amount between chemisorbed oxygen and ethanol. At the middle temperature (100 °C < T < 300 °C), the charged species is O^-.[26,27] The O^- of high reactivity is consumed once it meets the ethanol gas, which makes the ethanol sensor exhibit the high response. Although O^{2-} has high reactivity at high temperature, desorption of chemisorbed oxygen is dominated. The response is decreased. The operating temperature of optimization is 250 °C.

The schematic diagram represents the TENG treatment on the ZnO NMW sensor (Figure 2a). The frictional layers are the aluminum foil and Kapton layer. The output voltage of 300 V from TENG is applied on the ZnO NMW sensor after rectification. The frequency is 1 Hz. The photograph of the experiment setup of TENG treatment is shown in Figure S2. The output voltage curves before and after rectification are shown in Figure S3. The applied voltage on the ethanol sensor of ZnO NMW is about 26 V (Figure 2b). The current value at −2 V is increased as the treatment times increase (Figure S4). SBH decreases from 0.800 to 0.781 eV (Figure 2c). When the treatment times reach up to the 100, the response of 100 ppm ethanol is increased from 4.8 to 19.8 (Figure 2d and e). Whereas, the response of the ethanol sensor remains stable when the treatment times are over 100.

Schottky contact is formed between Ag and n-type ZnO NMW (Figure 3a). In a previous study, the oxygen vacancies in ZnO NMW could be driven to move along the c-axis under a high-intensity electric field.[28] Meanwhile, the high-intensity

electric field generated by TENG can drive the diffusion of oxygen vacancies in ZnO NMW toward to junction around the interface, which leads to the decrease of SBH. The phenomenon of polarization happens after TENG treatment because of the accumulation of oxygen vacancies (Figure 3b). The change of current and SBH can be expressed according to the formula as follows.

For the Ag-ZnO NMW Schottky junction after TENG treatment, the built-in potential φ_{bi} is given by

$$\varphi_{bi} = \frac{q}{2\varepsilon_s}(\rho_{polar}W_{polar}^2 + N_D W_{Dn}^2) \tag{1}$$

where q is the element charge, ε_s is the permittivity of ZnO, N_D is the donor concentration, and ρ_{polar} and W_{polar} are the polarization charges density and the distribution width of oxygen vacancies, respectively, which are functions of time that gradually build up as the TENG bias is applied. W_{Dn} is the width of depletion region on the n-type semiconductor.

The total current density of the Ag-ZnO NMW Schottky junction after polarizations can be given by[12,29]

$$J = J_0 \exp\left(\frac{q^2\rho_{polar}W_{polar}^2}{2\varepsilon_s k_B T}\right)\left[\exp\left(\frac{qV}{k_B T}\right) - 1\right] \tag{2}$$

where V is the bias voltage, k_B and T are the Boltzmann constant and temperature, respectively, J_0 is the saturation current density, and ε_s is the permittivity of ZnO.

For the M-S contact, J_0 is given by

$$J_0 = \frac{q^2 D_n N_c}{k_B T}\sqrt{\frac{2qN_D(\varphi_{bi0} - V)}{\varepsilon_s}}\exp\left(-\frac{q\phi_{Bn0}}{k_B T}\right) \tag{3}$$

where N_c and D_n are the effective density of states at the conduction band and electron diffusion coefficients, respectively, and ϕ_{Bn0} and φ_{bi0} are SBH and built-in potential without polarization charges.

After the polarization, the SBH of the ethanol sensor can be expressed as

$$\phi_{Bn} = \phi_{Bn0} - \frac{q\rho_{polar}W_{polar}^2}{2\varepsilon_s} \tag{4}$$

The response of the ZnO ethanol sensor from 5 to 200 ppm was measured. The response value of the initial sensor increases as the ethanol concentration increases (Figure 4a).
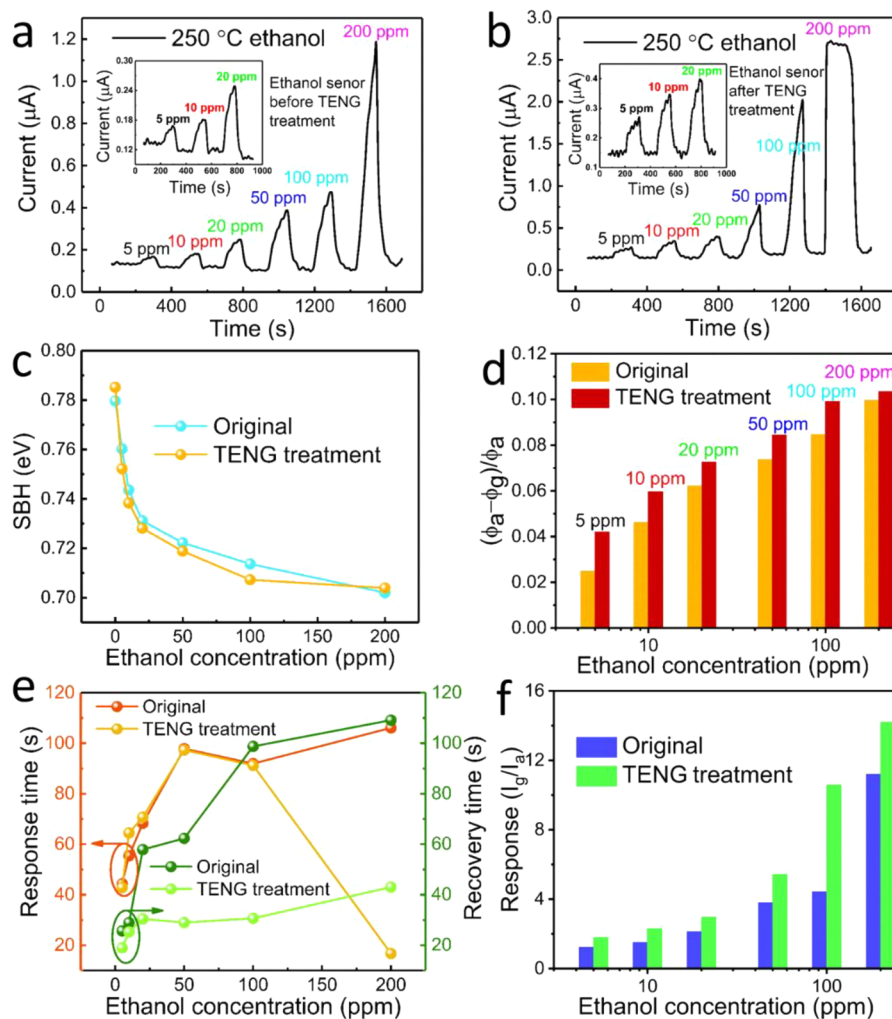
Figure 4. Response curve and the response of the ethanol sensor before and after TENG treatment. (a) Response curve of the initial sensor for the ethanol concentration from 5 to 200 ppm. (b) Response curve of the sensor after TENG treatment for an ethanol concentration from 5 to 200 ppm. (c) The SBH change of the ethanol sensor before and after TENG treatment as a function of ethanol concentration. (d) The change amount of SBH of the ethanol sensor before and after TENG treatment. (e) Response time and recovery time of the ethanol sensor before and after TENG treatment. (f) Response (I_g/I_a) of the ethanol sensor before and after TENG treatment.

The same phenomenon is also observed in the sensor after TENG treatment (Figure 4b). SBHs of the initial sensor before and after TENG treatment decrease with the ethanol concentration increase (Figure 4c). Whereas, the lowering amount of SBH to the sensor treated by TENG is greater than that of the initial sensor (Figure 4d). The change amount of current at 2 V also exhibits the same phenomenon (Figure S5). The response time has little change for the sensor before and after TENG treatment, and the recovery time is accelerated (Figure 4e), especially for the ethanol concentration over 10 ppm. The native point defects of oxygen vacancies are generated in ZnO inevitably during the preparation of ZnO nanowire.[30,31] The oxygen vacancies in the ZnO nanowire create the localized defect states. An external-electric-field-induced electrical potential will be proportionally and directly converted into the energy gains in ZnO nanowire. The gain in energy can be stored as the separation of a hole and electron in the defect of the oxygen vacancies. Then, the oxygen vacancy (V_O^0) will be converted into an ionized oxygen vacancy ((V_O^+) or (V_O^{2+})).[31,32] Ionized oxygen vacancies migrate toward the interface of the metal and semiconductor and the surface of the semiconductor when an external electric field is applied. The

accumulation of ionized oxygen vacancies with high oxidability and high energy on the interface and surface will increase the degree of surface reduction (number of oxygen vacancies).[33] If oxygen is present, the sufficient oxygen vacancies will accelerate the absorption of oxygen at the oxygen vacancies, which results in the decrease in conductivity quickly. The recovery time of the ethanol sensor after TENG treatment is shortened. In the case of an ethanol concentration of 200 ppm, the response of the gas sensor after TENG treatment is fast because lowering the amount of SBH reaches to saturation quickly. The response is calculated by I_g/I_a, where I_g is the current after exposing the sensor to the target gas and I_a is initial current in the air. The response of the sensor after TENG treatment is improved compared to that of the initial sensor (Figure 4f).

Once the n-type semiconductor is in air or ambient oxygen, the strong electron-drawing oxygen absorbed on ZnO NMW accepts the electrons from ZnO NMW. The negatively charged chemisorbed oxygen is formed in the depletion region and on the ZnO surface (Figure 5a). SBH is increased due to the negatively charged oxygen that absorbs at the depletion region and around it. Once the ethanol molecules meet the
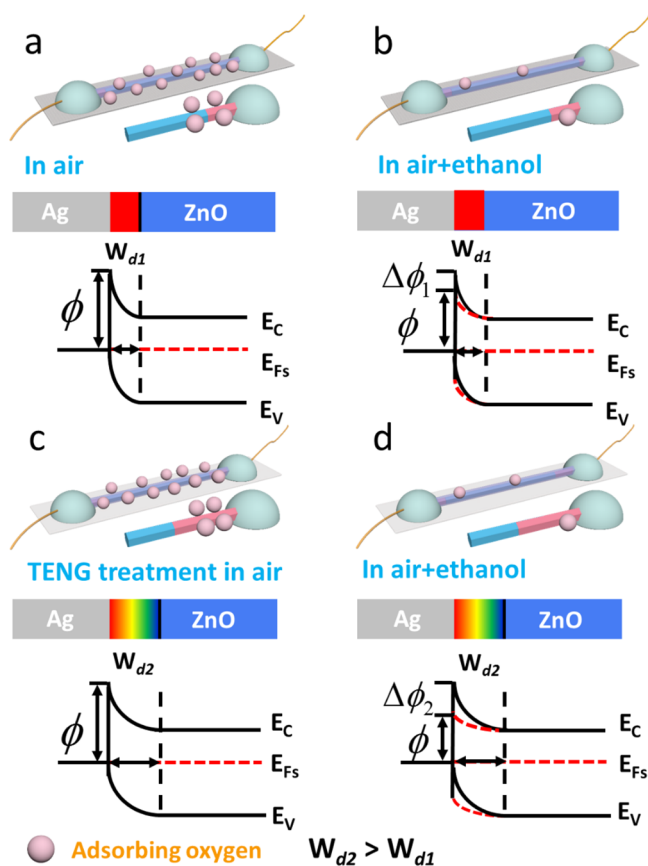
Figure 5. Proposed detection process of the ethanol sensor before and after TENG treatment. (a) Ethanol sensor before TENG treatment in ambient air. (b) Ethanol sensor before TENG treatment in the ambient air and ethanol. (c) Ethanol sensor after TENG treatment in ambient air. (d) Ethanol sensor after TENG treatment in ambient air and ethanol.

chemisorbed oxygen with high reaction activity, the chemisorb oxygen with a negative charge in the depletion region react with the ethanol molecules. SBH is lowered (Figure 5b). The current of the sensor is increased.

The high voltage applied on the ZnO NMW leads to the aggregation of oxygen vacancies on the junction around the interface. It is equivalent to applying the reverse voltage on the Schottky junction. The width of the depletion region is increased according to[34,35]

$$W_D = \sqrt{\frac{2\varepsilon_s}{qN_D}\left(V_{bi} - V - \frac{k_B T}{q}\right)} \tag{5}$$

where W_D is the width of the depletion region, and the other parameters in this formula are the same as in eq 3. The sign of V is positive for forward bias and negative for reverse bias.

The width of the depletion region is increased after TENG treatment (Figure 5c). More oxygen molecules can be absorbed in the depletion region (Figure 5c). When the ethanol molecules meet the chemisorbed oxygen in the depletion region, more chemisorbed oxygen is consumed. The lowering amount of SBH is greater than that of the initial sensor (Figure 5d), allowing more carrier to pass through the metal−semiconductor junction. The response current is enhanced, and the response (I_g/I_a) of ethanol is improved.

■ CONCLUSION

A highly sensitive ethanol sensor combined with the ZnO NMW Schottky junction and TENG was developed and investigated. The ideality factors of source and drain electrodes are decreased as the work temperature increases, whereas the SBH is increased. An interesting phenomenon is found where SBH of the ethanol sensor based on ZnO (n-type) can be lowered by the impact of positive voltage generated by TENG. The diffusion of oxygen vacancies driven by the high intensity electric field generated by the high voltage from TENG makes them aggregate at the junction around the interface. It is equivalent to applying the reverse voltage on the Schottky junction. The increase of depletion width leads to more chemisorbed oxygen being consumed in the depletion region after injecting the ethanol gas. The greater lowering amount of SBH makes the response of the ethanol sensor increase. The response of the ethanol sensor is enhanced by 139% for 100 ppm ethanol after TENG treatment of 100 times. The recovery time is shortened. This study provides a new, simple, and effective method to improve the sensor sensitivity.

■ EXPERIMENTAL SECTION

ZnO NMWs were fabricated by the vapor−solid growth process. The ZnO powder (3 g, 99.99% purity) as the precursor was mixed with activated carbon powder (3 g, 99.99% purity) uniformly. The mixture was transferred to an alumina boat. The single-crystal silicon wafer (Si(100)) as the substrate was ultrasonically cleaned in acetone and ethanol for 10 min each, respectively. The silicon substrate is placed on top of the alumina boat horizontally. Then, the alumina boat was placed in the center of the tube furnace. The synthesis process was conducted at a temperature of 1050 °C for 40 min. During the reaction, argon and oxygen were utilized as the carrier gases. The argon-to-oxygen ratio was 10:1.

An individual ZnO NMW was transferred to the glass substrate. The silver paste was used to fix both ends. It was also used as the electrode connected with the Cu conducting wire. The high-temperature resistant adhesive was coated on the surface of the silver paste to improve the adhesive force between the substrate and silver paste.

The acrylic with the thickness of 4 mm was used as the robust substrate. The aluminum foil and kapton membrane which were fixed on the acrylic were the friction layer. The surfaces of Al foil and kapton film were polished by sandpaper. The 50 nm Cu film deposited by the magnetron sputtering was used as the back electrode.

The measurement of gas sensing was carried out in the sealed chamber with a volume of 18 L. The gas sensor based on the ZnO NMW was preheated for 30 min to ensure that the resistance was stable. Ethanol was injected into the evaporator at a temperature of 170 °C. The gasified ethanol was distributed in the whole chamber dynamically. The ethanol gas was pumped to recover the status in the air. The testing time was 2 min. The current change was measured by using the Keithley 6517 system. The applied bias was 2 V. Data were captured by using a Tektronix oscilloscope (type: HD06104). The $I−V$ curve ranged from −2 to 2 V and was conducted on the semiconductor characterization system (Keithley 4200-SCS).

■ ASSOCIATED CONTENT

⒮ Supporting Information

The Supporting Information is available free of charge at https://pubs.acs.org/doi/10.1021/acs.nanolett.0c01063.

Response and recovery curves of the ZnO ethanol sensor at 100 ppm as a function of temperature, photograph of the experiment setup of TENG treatment, the output voltage of the TENG before and after rectification, the $I-V$ curve of the ZnO NMW ethanol sensor as a function of treatment times by TENG at 250 °C, and $I-V$ curve before and after TENG treatment for different concentrations of ethanol at 250 °C (PDF)

■ AUTHOR INFORMATION

Corresponding Author

Zhou Li − *CAS Center for Excellence in Nanoscience, Beijing Institute of Nanoenergy and Nanosystems, Chinese Academy of Sciences, Beijing 100083, P.R. China; School of Nanoscience and Technology, University of Chinese Academy of Sciences, Beijing 100049, P.R. China; Center on Nanoenergy Research, School of Physical Science and Technology, Guangxi University, Nanning 530004, P.R. China;* ⓘ orcid.org/0000-0002-9952-7296; Email: zli@binn.cas.cn

Authors

Jianping Meng − *CAS Center for Excellence in Nanoscience, Beijing Institute of Nanoenergy and Nanosystems, Chinese Academy of Sciences, Beijing 100083, P.R. China*

Hu Li − *CAS Center for Excellence in Nanoscience, Beijing Institute of Nanoenergy and Nanosystems, Chinese Academy of Sciences, Beijing 100083, P.R. China; Beijing Advanced Innovation Centre for Biomedical Engineering, Key Laboratory for Biomechanics and Mechanobiology of Chinese Education Ministry, School of Biological Science and Medical Engineering, Beihang University, Beijing 100191, P.R. China*

Luming Zhao − *CAS Center for Excellence in Nanoscience, Beijing Institute of Nanoenergy and Nanosystems, Chinese Academy of Sciences, Beijing 100083, P.R. China; School of Nanoscience and Technology, University of Chinese Academy of Sciences, Beijing 100049, P.R. China*

Junfeng Lu − *CAS Center for Excellence in Nanoscience, Beijing Institute of Nanoenergy and Nanosystems, Chinese Academy of Sciences, Beijing 100083, P.R. China*

Caofeng Pan − *CAS Center for Excellence in Nanoscience, Beijing Institute of Nanoenergy and Nanosystems, Chinese Academy of Sciences, Beijing 100083, P.R. China; School of Nanoscience and Technology, University of Chinese Academy of Sciences, Beijing 100049, P.R. China; Center on Nanoenergy Research, School of Physical Science and Technology, Guangxi University, Nanning 530004, P.R. China;* ⓘ orcid.org/0000-0001-6327-9692

Yan Zhang − *CAS Center for Excellence in Nanoscience, Beijing Institute of Nanoenergy and Nanosystems, Chinese Academy of Sciences, Beijing 100083, P.R. China; School of Physics, University of Electronic Science and Technology of China, Chengdu 610054, P.R. China;* ⓘ orcid.org/0000-0002-7329-0382

Complete contact information is available at:
https://pubs.acs.org/10.1021/acs.nanolett.0c01063

Author Contributions

▽J.P. Meng and H. Li contributed equally to this work.

Notes

The authors declare no competing financial interest.

■ ACKNOWLEDGMENTS

■ REFERENCES

(1) Wen, Z.; Chen, J.; Yeh, M. H.; Guo, H.; Li, Z.; Fan, X.; Zhang, T.; Zhu, L.; Wang, Z. L. Blow-driven triboelectric nanogenerator as an active alcohol breath analyzer. *Nano Energy* **2015**, *16*, 38−46.

(2) Naderinasrabadi, M.; Mortazavi, Y.; Khodadadi, A. A. Highly sensitive and selective Gd2O3-doped SnO2 ethanol sensors synthesized by a high temperature and pressure solvothermal method in a microreactor. *Sens. Actuators, B* **2016**, *230*, 130−139.

(3) Ho, J. J.; Fang, Y. K.; Wu, K. H.; Hsieh, W. T.; Chen, C. H.; Chen, G. S.; Ju, M. S.; Lin, J. J.; Hwang, S. B. High sensitivity ethanol gas sensor integrated with a solid-state heater and thermal isolation improvement structure for legal drink-drive limit detecting. *Sens. Actuators, B* **1998**, *50*, 227−233.

(4) Tricoli, A.; Righettoni, M.; Teleki, A. Semiconductor gas sensors: dry synthesis and application. *Angew. Chem., Int. Ed.* **2010**, *49*, 7632−7659.

(5) Zhang, J.; Liu, X.; Neri, G.; Pinna, N. Nanostructured Materials for Room-Temperature Gas Sensors. *Adv. Mater.* **2016**, *28*, 795−831.

(6) Hu, Y. F.; Zhou, J.; Yeh, P.-H.; Li, Z.; Wei, T.-Y.; Wang, Z. L. Supersensitive, Fast-Response Nanowire Sensors by Using Schottky Contacts. *Adv. Mater.* **2010**, *22*, 3327−3332.

(7) Yu, R. M.; Niu, S. M.; Pan, C. F.; Wang, Z. L. Piezotronic effect enhanced performance of Schottky-contacted optical, gas, chemical and biological nanosensors. *Nano Energy* **2015**, *14*, 312−339.

(8) Wei, T.-Y.; Yeh, P.-H.; Lu, S.-Y.; Wang, Z. L. Gigantic Enhancement in Sensitivity Using Schottky Contacted Nanowire Nanosensor. *J. Am. Chem. Soc.* **2009**, *131*, 17690−17695.

(9) Niu, S.; Hu, Y.; Wen, X.; Zhou, Y.; Zhang, F.; Lin, L.; Wang, S.; Wang, Z. L. Enhanced Performance of Flexible ZnO Nanowire Based Room-Temperature Oxygen Sensors by Piezotronic Effect. *Adv. Mater.* **2013**, *25*, 3701−3706.

(10) Fu, Y.; Zang, W.; Wang, P.; Xing, L.; Xue, X.; Zhang, Y. Portable room-temperature self-powered/active H₂ sensor driven by human motion through piezoelectric screening effect. *Nano Energy* **2014**, *8*, 34−43.

(11) Zhao, L. M.; Li, H.; Meng, J. P.; Wang, A. C.; Tan, P. C.; Zou, Y.; Yuan, Z. Q.; Lu, J. F.; Pan, C. F.; Fan, Y. B.; Zhang, Y. M.; Zhang, Y.; Wang, Z. L.; Li, Z. Reversible Conversion between Schottky and Ohmic Contacts for Highly Sensitive, Multifunctional Biosensors. *Adv. Funct. Mater.* **2020**, *30*, 1907999.

(12) Wang, Z. L.; Wu, W. Piezotronics and piezo-phototronics: fundamentals and applications. *Nat. Sci. Rev.* **2014**, *1*, 62−90.

(13) Dong, Y.; Brillson, L. J. First-Principles Studies of Metal (111)/ ZnO{0001} Interfaces. *J. Electron. Mater.* **2008**, *37*, 743−748.

(14) Pan, C. F.; Zhai, J. Y.; Wang, Z. L. Piezotronics and Piezo-phototronics of Third Generation Semiconductor Nanowires. *Chem. Rev.* **2019**, *119*, 9303−9359.

(15) Liu, W.; Zhang, A.; Zhang, Y.; Lin Wang, Z. First principle simulations of piezotronic transistors. *Nano Energy* **2015**, *14*, 355−363.

(16) Wu, C.; Wang, A. C.; Ding, W.; Guo, H.; Wang, Z. L. Triboelectric Nanogenerator: A Foundation of the Energy for the New Era. *Adv. Energy Mater.* **2019**, *9*, 1802906.

(17) Wang, Z. L. Triboelectric nanogenerators as new energy technology for self-powered systems and as active mechanical and chemical sensors. *ACS Nano* **2013**, *7*, 9533.

(18) Wang, Z. L. On Maxwell's displacement current for energy and sensors: the origin of nanogenerators. *Mater. Today* **2017**, *20*, 74−82.

(19) Shi, B. J.; Liu, Z.; Zheng, Q.; Meng, J. P.; Ouyang, H.; Zou, Y.; Jiang, D. J.; Qu, X. C.; Yu, M.; Zhao, L. M.; Fan, Y. B.; Wang, Z. L.; Li, Z. Body-Integrated Self-Powered System for Wearable and Implantable Applications. *ACS Nano* **2019**, *13*, 6017−6024.

(20) Zou, Y.; Tan, P. C.; Shi, B. J.; Ouyang, H.; Jiang, D. J.; Liu, Z.; Li, H.; Yu, M.; Wang, C.; Qu, X. C.; Zhao, L. M.; Fan, Y. B.; Wang, Z. L.; Li, Z. A bionic stretchable nanogenerator for underwater sensing and energy harvesting. *Nat. Commun.* **2019**, *10*, 1−10.

(21) Nam, C. Y.; Tham, D.; Fischer, J. E. Disorder effects in focused-ion-beam-deposited Pt contacts on GaN nanowires. *Nano Lett.* **2005**, *5*, 2029−2033.

(22) Das, S. N.; Choi, J. H.; Kar, J. P.; Moon, K. J.; Lee, T. I.; Myoung, J. M. Junction properties of Au/ZnO single nanowire Schottky diode. *Appl. Phys. Lett.* **2010**, *96*, 092111.

(23) Hu, Y.; Klein, B. D.; Su, Y.; Niu, S.; Liu, Y.; Wang, Z. L. Temperature dependence of the piezotronic effect in ZnO nanowires. *Nano Lett.* **2013**, *13*, 5026−5032.

(24) Park, C. O.; Akbar, S. A. Ceramics for chemical sensing. *J. Mater. Sci.* **2003**, *38*, 4611−4637.

(25) Wen, Z.; Zhu, L. P.; Li, Y. G.; Zhang, Z. Y.; Ye, Z. Z. Mesoporous Co_3O_4 nanoneedle arrays for high-performance gas sensor. *Sens. Actuators, B* **2014**, *203*, 873−879.

(26) Barsan, N.; Weimar, U. Conduction Model of Metal Oxide Gas Sensors. *J. Electroceram.* **2001**, *7*, 143−167.

(27) Li, W. Y.; Xu, L. N.; Chen, J. Co_3O_4 nanomaterials in lithium-ion batteries and gas sensors. *Adv. Funct. Mater.* **2005**, *15*, 851−857.

(28) Ding, Y.; Liu, Y.; Niu, S. M.; Wu, W. Z.; Wang, Z. L. Pyroelectric-field driven defects diffusion along c-axis in ZnO nanobelts under high-energy electron beam irradiation. *J. Appl. Phys.* **2014**, *116*, 154304.

(29) Zhang, Y.; Liu, Y.; Wang, Z. L. Fundamental Theory of Piezotronics. *Adv. Mater.* **2011**, *23*, 3004−3013.

(30) Janotti, A.; Van de Walle, C. G. Native point defects in ZnO. *Phys. Rev. B: Condens. Matter Mater. Phys.* **2007**, *76*, 165202.

(31) Lany, S.; Zunger, A. Anion vacancies as a source of persistent photoconductivity in II-VI and chalcopyrite semiconductors. *Phys. Rev. B: Condens. Matter Mater. Phys.* **2005**, *72*, 035215.

(32) Huang, B. L.; Sun, M. Z.; Peng, D. F. Intrinsic energy conversions for photon-generation in piezo-phototronic materials: A case study on alkaline niobates. *Nano Energy* **2018**, *47*, 150−171.

(33) Gurlo, A.; Riedel, R. In situ and operando spectroscopy for assessing mechanisms of gas sensing. *Angew. Chem., Int. Ed.* **2007**, *46*, 3826−3848.

(34) Zhang, Z. Y.; Yao, K.; Liu, Y.; Jin, C. H.; Liang, X. L.; Chen, Q.; Peng, L. M. Quantitative analysis of current-voltage characteristics of semiconducting nanowires: Decoupling of contact effects. *Adv. Funct. Mater.* **2007**, *17*, 2478−2489.

(35) Liu, Y.; Zhang, Z. Y.; Hu, Y. F.; Jin, C. H.; Peng, L. M. Quantitative fitting of nonlinear current-voltage curves and parameter retrieval of semiconducting nanowire, nanotube and nanoribbon devices. *J. Nanosci. Nanotechnol.* **2008**, *8*, 252−258.